

1 **Measurement Report: Wintertime new particle formation in the rural area of North**  
2 **China Plain: influencing factors and possible formation mechanism**

3  
4  
5 **Juan Hong<sup>1,2†\*</sup>, Min Tang<sup>1,2†</sup>, Qiaoqiao Wang<sup>1,2\*</sup>, Nan Ma<sup>1,2</sup>, Shaowen Zhu<sup>1,2</sup>, Shaobin**  
6 **Zhang<sup>1,2</sup>, Xihao Pan<sup>1,2</sup>, Linhong Xie<sup>1,2</sup>, Guo Li<sup>3</sup>, Uwe Kuhn<sup>3</sup>, Chao Yan<sup>4</sup>, Jiangchuan**  
7 **Tao<sup>1,2</sup>, Ye Kuang<sup>1,2</sup>, Yao He<sup>1,2</sup>, Wanyun Xu<sup>5</sup>, Runlong Cai<sup>6</sup>, Yaqing Zhou<sup>1,2</sup>, Zhibin**  
8 **Wang<sup>7</sup>, Guangsheng Zhou<sup>5</sup>, Bin Yuan<sup>1</sup>, Yafang Cheng<sup>3</sup>, Hang Su<sup>3</sup>**  
9

10 <sup>1</sup>Institute for Environmental and Climate Research, Jinan University, Guangzhou, Guangdong  
11 511443, China

12 <sup>2</sup>Guangdong-Hongkong-Macau Joint Laboratory of Collaborative Innovation for Environmental  
13 Quality, Guangzhou, China

14 <sup>3</sup>Multiphase Chemistry Department, Max Planck Institute for Chemistry, Mainz 55128, Germany

15 <sup>4</sup>School of Atmospheric Sciences, Joint International Research Laboratory of Atmospheric and  
16 Earth System Sciences, Nanjing University, Nanjing, China

17 <sup>5</sup>Hebei Gucheng, Agrometeorology, National Observation and Research Station, Chinese Academy  
18 of Meteorological Sciences, Beijing, 100081, China

19 <sup>6</sup>Institute for Atmospheric and Earth System Research/Physics, Faculty of Science, University of  
20 Helsinki, Helsinki, FI00014, Finland

21 <sup>7</sup>College of Environmental and Resource Sciences, Zhejiang University, Zhejiang Provincial Key  
22 Laboratory of Organic Pollution Process and Control, Hangzhou 310058, China

23 <sup>†</sup>These authors contributed equally to this work.

24 \*Correspondence: Qiaoqiao Wang ([qwang@jnu.edu.cn](mailto:qwang@jnu.edu.cn)) and Juan Hong  
25 ([juanhong0108@jnu.edu.cn](mailto:juanhong0108@jnu.edu.cn))

26  
27 **Abstract:**

28 The high concentration of fine particles as well as gaseous pollutants makes  
29 polluted areas, such as the urban setting of North China Plain (NCP) of China, a  
30 different environment for NPF compared to many clean regions. Such conditions also  
31 hold for other polluted environments in this region, for instance, the rural area of  
32 NCP, yet the underlying mechanisms for NPF remain less understood owing to the  
33 limited observations of particles in the sub-3nm range. Comprehensive  
34 measurements, particularly covering the particle number size distribution down to  
35 1.3 nm, were conducted at a rural background site of Gucheng (GC) in the North  
36 China Plain (NCP) from 12 November to 24 December in 2018. Five NPF events  
37 during the 39 effective days of measurements for the campaign were identified, with

38 the mean particle nucleation rate ( $J_{1.3}$ ) and growth rate ( $GR_{1.3-2.4}$ ) were  $22.0 \text{ cm}^{-3}\cdot\text{s}^{-1}$   
39 and  $3.9 \text{ nm}\cdot\text{h}^{-1}$ , respectively. During these five days, NPF concurrently occurred at an  
40 urban site in Beijing. Sharing similar sources and transport paths of air masses  
41 arriving at our site to that of urban Beijing, we hypothesis that NPF events during  
42 these days in this region might be a regional phenomenon. The simultaneous  
43 occurrence of NPF in both places implies that  $\text{H}_2\text{SO}_4$ -amine nucleation, concluded for  
44 urban Beijing there, could probably be the dominating mechanism for NPF at our  
45 rural site. The higher concentration of sulfuric acid during many non-event days  
46 compared to that of event days indicates that the content of sulfuric acid may not  
47 necessarily lead to NPF events under current atmosphere. Only when the  
48 condensation sink or coagulation sink was significantly lowered, atmospheric NPF  
49 occurred, implying that CS or CoagS are the dominating factor controlling the  
50 occurrence of NPF for present rural environment of NCP, being quite similar to the  
51 feature at urban Beijing.

52

53 **Keywords:** new particle formation, particle number size distribution, condensational  
54 sink, nucleation mechanism.

## 55 **1. Introduction**

56 Atmospheric new particle formation (NPF) is a major source of the global  
57 particles in terms of number concentration and size distribution (Kulmala et al., 2004)  
58 and is considered to contribute up to half of the global cloud condensation nuclei  
59 (CCN) budget in the lower troposphere (Spracklen et al., 2006; Dunne et al., 2016). In  
60 general, NPF consists of two consecutive processes: a) the formation or nucleation of  
61 molecular clusters by low-volatile gaseous substances, and b) their subsequent  
62 growth to detectable sizes or even larger, at which these particles may act as CCN or  
63 contribute to the particle mass concentration (Kulmala et al., 2000; Zhang et al.,  
64 2012).

65 Numerous laboratory measurements and field studies have shown that sulfuric  
66 acid molecules ( $\text{H}_2\text{SO}_4$ ) are one of the key precursors to form molecular clusters for  
67 nucleation (Nieminen et al., 2010; Sipilä et al., 2010; Kirkby et al., 2011; Riccobono et  
68 al., 2014; Stolzenburg et al., 2020). However, these  $\text{H}_2\text{SO}_4$  clusters relevant to  
69 atmospheric nucleation are typically quite small, i.e., with diameters below 1.5 nm,  
70 at which the detection efficiency of traditional instruments specific for NPF was  
71 usually unsatisfactory (Kulmala et al., 2013). This had led to large uncertainties in the  
72 measured formation rate of newly formed particles and thus required precise  
73 measurements of these clusters or particles down to sub-3 nm. Upon recently,  
74 progress such as the use of a particle size magnifier (PSM) (Vanhanen et al., 2011;  
75 Xiao et al., 2015), a neutral cluster and air ion spectrometer (NAIS) (Mirme and  
76 Mirme, 2013) and a chemical ionization atmospheric pressure interface time-of-flight  
77 mass spectrometer (CI-API-TOF) (Jokinen et al., 2012) make it possible to directly  
78 measure the number concentration of clusters in the 1-3 nm size range. Benefit from  
79 these novel techniques, observations have found that the growth of  $\text{H}_2\text{SO}_4$  clusters  
80 would be significantly promoted after stabilized by other precursors like amines,  
81 ammonia or iodine species (Berndt et al., 2010; Kirkby et al., 2011; Almeida et al.,  
82 2013; Riccobono et al., 2014; Kürten et al., 2016; Sipilä et al., 2010). Furthermore,

83 oxidation products from volatile organic compounds, for instance, highly oxidized  
84 organic compounds, were suggested to be important contributors to atmospheric  
85 nucleation (Ehn et al., 2014; Bianchi et al., 2016; Kirkby et al., 2016; Tröstl et al.,  
86 2016).

87 The North China Plain (NCP) of China, has been suffering heavily from the highly  
88 complex air pollution since decades (Ma et al., 2016; Shen et al., 2018; Zhang et al.,  
89 2020), owing to the high emissions or formation of different pollutants such as SO<sub>2</sub>,  
90 NH<sub>3</sub>, VOCs as well as fine particles from various sources (Guo et al., 2014; Zhang et al.,  
91 2015). Due to the high concentration of pre-existing particles, previous studies  
92 considered that in the NCP, less NPF would occur as the newly-formed particles  
93 would be scavenged much faster before growing. By contrast, atmospheric NPF was  
94 still frequently observed in this region (Chu et al., 2019; Deng et al., 2020; Cai et al.,  
95 2021), being more often than theoretically predicted (Kulmala et al., 2014), indicating  
96 that the underlying mechanisms for NPF in this area might be different, that those  
97 mechanism previously found for other environments might not be completely  
98 applicable. The higher concentration of these gaseous precursors makes this region  
99 an unique condition for NPF compared to relatively clean environments (Kulmama et  
100 al., 2016; Yu et al., 2017; Wang et al., 2017), further supporting the hypothesis of  
101 different formation mechanisms and thereby distinct features of NPF events in this  
102 region. These doubts concerning NPF in the NCP, however, still remain to be  
103 elucidated due to limitations of comprehensive measurements, particularly for rural  
104 areas of the NCP, where observations regarding NPF was even more rare.

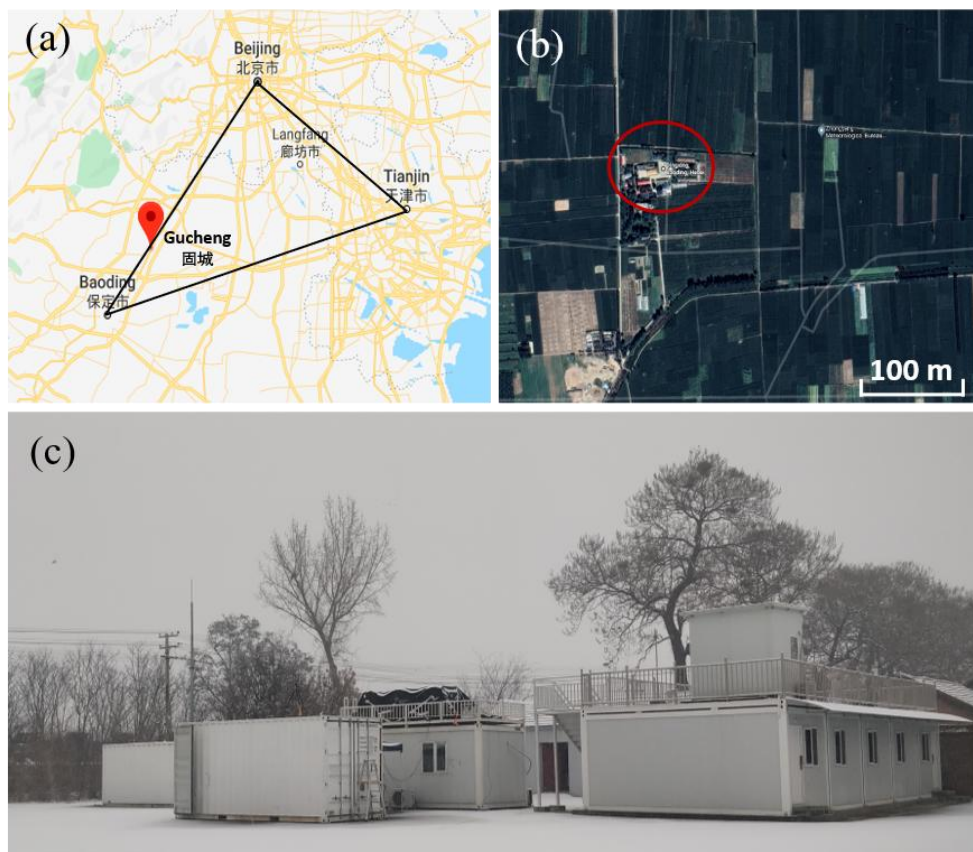
105 In addition, with respect to those existing studies concerning NPF in the NCP,  
106 they mainly focused on the measurements of particles beyond 3 nm. Without  
107 applicable instruments, observations of new particles down to sub-3nm was still  
108 quite limited (Fang et al., (2020); Zhou et al., (2020)), causing large uncertainties in  
109 the measured characteristics of NPF for current region. To fill the gap of  
110 measurements of particles or clusters in the size range of 1-3 nm and further  
111 advance our understanding of NPF in this region, particularly in the rural area of NCP,  
112 we conducted a comprehensive measurement campaign at a rural background site in

113 the NCP during 12 November to 24 December, 2018. By obtaining the particle  
114 number size distribution over a wide diameter range (1.3 nm - 10  $\mu$ m), we aimed to  
115 investigate the characteristics of NPF events at the rural site in NCP during  
116 wintertime, find out which factors govern the occurring of NPF compared to other  
117 regions of NCP such as the urban areas and explore the potential mechanisms for  
118 NPF in this area.

119 **2. Experiment**

120 **2.1. Field measurements site**

121 The measurements were conducted at Gucheng (GC) site ( $39^{\circ}09'01.1''\text{N}$   
122  $115^{\circ}44'02.6''\text{E}$ ), situated at an Ecological and Agricultural Meteorology Station  
123 ( $39^{\circ}09' \text{ N}$ ,  $115^{\circ}44' \text{ E}$ ) of the Chinese Academy of Meteorological Sciences from 12  
124 November to 24 December in 2018. The station is located in Dingxing county,  
125 Baoding city, Hebei Province, China, as seen in Fig.1 and surrounded by agricultural  
126 fields and sporadic villages. Being far from the urban and industrial emission areas,  
127 this site can be treated as a representative regional site in the northern part of NCP.  
128 More details about this site can be found in Lin et al. (2009) and Shen et al. (2018).



129  
130 Figure 1. The upper panel shows the geographical location of the site (red dot and circled, ©  
131 Google Maps), where our field measurements were carried out. The lower panel shows the  
132 measurement containers, where the sampling instruments were set up.

## 133 **2.2. Measurements**

### 134 **2.2.1. Particle Number Size Distribution (PNSD) measurement**

135 The aerosol sampling inlet was located on the rooftop of a measurement  
136 container, where room temperature was maintained at 22 °C (Fig1. c). The aerosol  
137 was sampled via a low-flow PM<sub>10</sub> cyclone inlet, passed through a Nafion dryer, and  
138 directed to different instruments through stainless steel or conductive black tubings  
139 using an isokinetic flow splitter. The particle number size distribution of aerosol  
140 particles with diameters from 10 nm to 10000 nm was measured by using a scanning  
141 mobility particle sizer (SMPS, model TSI 3938) and an Aerodynamic Particle Size  
142 Spectrometer (APS, model TSI 3321) at a time resolution of around 5 minutes. The  
143 SMPS consisted of an electrostatic classifier (model TSI 3080) and a condensation  
144 particle counter (CPC, model TSI 3772).

### 145 **2.2.2. Sub-3nm Particle Number Concentration measurement**

146 Sub-3nm particles were measured with an Airmodus nano Condensation  
147 Nucleus Counter system (nCNC, model A11), consisting of a Particle Size Magnifier  
148 (PSM, model A10) and a butanol condensation particle counter (CPC, model A20)  
149 (Vanhanen et al., 2011). The Airmodus PSM uses diethylene glycol as the working  
150 fluid to activate and grow nano-sized particles. Specifically, the PSM was operated  
151 under the scanning mode that the diethylene glycol flow was varied between 0.1 to  
152 1.3 L·min<sup>-1</sup>. Thus, the number size distribution of five different size bins, i.e., 1.3-1.4,  
153 1.4-1.6, 1.6-1.9, 1.9-2.4, and 2.4-3.7 nm was obtained. Owing to the data quality,  
154 only the former four size bins data were used in this study. During this campaign, the  
155 duration of each scan was completed within around 240 s.

### 156 **2.2.3. Pollutant gases, PM<sub>2.5</sub> and meteorological parameters measurement**

157 Concentration of trace gases, including SO<sub>2</sub>, O<sub>3</sub>, CO and NO<sub>x</sub>, was measured  
158 continuously during this campaign using different Thermo Fisher Analysers (model

159 43i-TLE, 49i, 48i, and 42i), respectively, at a time resolution of 1 minute. The  
160 concentration of oxygenated volatile organic compounds (OVOCs) was measured  
161 with an iodide-adduct long time-of-flight chemical ionization mass spectrometer  
162 (I-CIMS, Aerodyne, US) at a time resolution of 10-30 s for current study.

163 In addition, ambient meteorological conditions, such as wind speed, wind  
164 direction, temperature, relative humidity and solar radiation, were also regularly  
165 measured in another building, which is located about 20 meters to the southwest of  
166 the container, at the same observational site.

167 Furthermore, in order to investigate the influence of the origins and transport  
168 paths of air parcels to the local atmospheric compositions during NPF events, 72-h  
169 back trajectories of air masses arriving at 100 m above ground level at our GC site  
170 were analyzed using the HYbrid Single-Particle Lagrangian Integrated Trajectory  
171 (HYSPLIT) model for the classified event days.

## 172 **2.3. Data processing**

### 173 **2.3.1. Formation Rate ( $J_{D_p}$ ) and Growth Rate ( $GR$ )**

174  $J_{D_p}$  defines the formation rate of atmospheric particles at a certain diameter ( $D_p$ )  
175 and can be calculated according to Kulmala et al. (2012) as:

$$J_{D_p} = \frac{dN_{\Delta D_p}}{dt} + CoagS_{\Delta D_p} \times N_{\Delta D_p} + \frac{1}{\Delta D_p} GR_{\Delta D_p} \times N_{\Delta D_p}$$

176 where  $N$  is the particle number concentration between the diameter  $dp_2$  and  $dp_1$   
177 (denotes as  $\Delta D_p$ ),  $CoagS$  is the coagulation sink of particles,  $GR$  is the particle  
178 growth rate out of the selected size bin.

179 In our study, we used two independent methods to calculate GR. One is the  
180 maximum concentration method (Kulmala et al., 2012), being mainly for the PSM  
181 data. The other is based on the variation in geometric mean diameters of particle  
182 number size distribution, which is derived by fitting the PNSD into 2 or 3 log-normal  
183 modes using an automatic algorithm (DO-FIT model) (Hussein et al., 2005), mainly for  
184 SMPS data.



$$GR = \frac{ddp}{dt} = \frac{\Delta dp}{\Delta t} = \frac{dp_2 - dp_1}{t_2 - t_1}$$

185 where  $dp_1$  and  $dp_2$  were particle diameters at time  $t_1$  and  $t_2$ , respectively.

### 186 2.3.2. Condensation Sink (CS) and Coagulation Sink (CoagS)

187 CS describes how fast the low-volatility molecules condense onto pre-existing  
188 aerosols and can be expressed as (Kulmala et al., 2012):

$$CS = 2\pi D \int_0^{dp_{max}} \beta_{m,dp} dp N_{dp} ddp = 2\pi D \sum_{dp} \beta_{m,dp} dp N_{dp}$$

189 where  $D$  is the diffusion coefficient of the condensing vapor, which is usually referred  
190 to sulfuric acid and  $\beta_{m,dp}$  is the mass flux transition correction factor.

191 CoagS represents how fast the freshly formed particles are lost to pre-existing  
192 particles through coagulation and can be calculated as :

$$CoagS_{dp} = \int K(dp, dp') n(dp) ddp' \cong \sum_{dp'=dp}^{dp'=max} K(dp, dp') N_{dp'}$$

193 where,  $K(dp, dp')$  is the collision efficiency between particles at the diameter from  
194  $dp$  to  $dp'$ .

### 195 2.3.3. Sulfuric Acid proxy (SA proxy)

196 SA was considered as one of the key precursors responsible for particle  
197 nucleation in the atmosphere. However, no direct measurement for the  
198 concentration of SA was available in current study. We therefore used a proxy  
199 variable to substitute the concentration of SA, as SA is mainly produced by the  
200 oxidation of  $SO_2$  by OH radicals, which can be approximated by the UV-B intensity  
201 (Petäjä et al., 2009). Thus, the proxy concentration of SA can be calculated by Lu et al.  
202 (2019):

$$203 SA \text{ proxy} = 0.0013 \cdot UVB^{0.13} \cdot [SO_2]^{0.40} \cdot CS^{-0.17} \cdot ([O_3]^{0.44} + [NO_x]^{0.41})$$

#### 204 **2.3.4. Classification of NPF event**

205 Days of NPF events was classified according to the method proposed by Dal  
206 Maso et al. (2005) and Kulmala et al. (2012), in which (a) a burst in the concentration  
207 of sub-3 nm particles or clusters was observed and (b) these particles had a  
208 continuous growth over a time span of hours (e.g., usually more than ten hours). If  
209 no clear growth of these newly formed particles (sub-3 nm particles) can be  
210 identified, the day was classified as an undefined day. The day without both the  
211 burst of sub-3 nm particles and their subsequent growth was considered as a  
212 non-event day.

#### 213 **2.3.5. Indicator for the occurrence of NPF**

214 Previously, McMurry et al. (2005) proposed a dimensionless criterion,  $L$ , to  
215 predict the occurrence of NPF events in the atmosphere. After being validated in  
216 diverse atmospheric environments (Kuang et al., 2010; Cai et al., 2017),  $L$  has been  
217 used to investigate the governing factors for NPF events under typical atmospheric  
218 conditions. Upon recently, Cai et al. (2021a) proposed a new indicator,  $I$ , on the basis  
219 of  $L$ , which only considered  $\text{H}_2\text{SO}_4$  to drive the growth. The new indicator was  
220 calculated by further taking into account the condensation of other species, for  
221 instance, amines and has been suggested to be a good quantitative representation  
222 for the occurrence of NPF after comparing with  $L$  for NPF events observed at urban  
223 Beijing (Deng et al., 2020). The detailed information to calculate  $I$  can be found in  
224 (Cai et al., 2021a).

## 225 **3. Results and discussion**

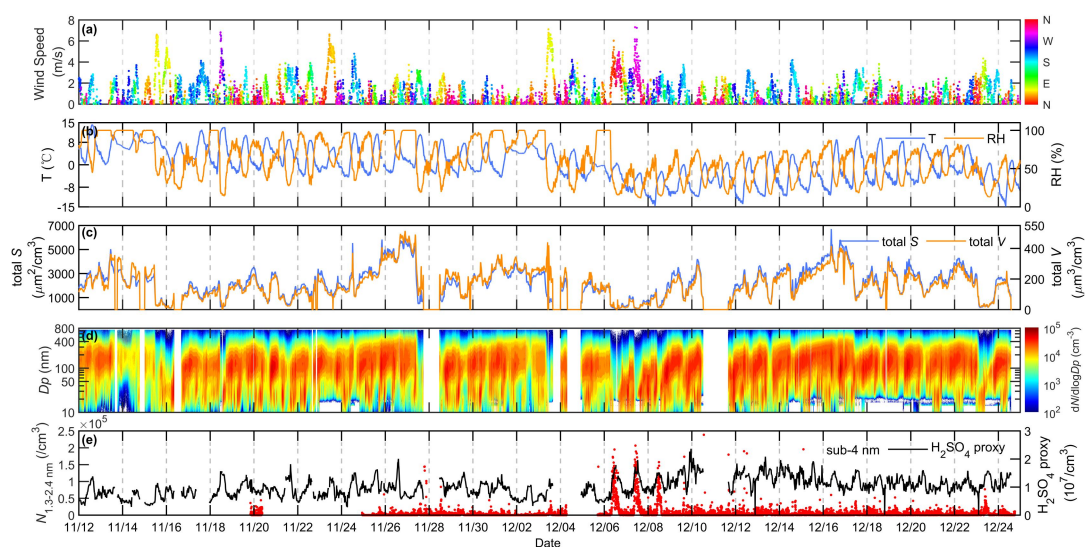
### 226 **3.1. General characteristics of NPF at GC site**

227 Figure 2 shows the time series of meteorological parameters (a: wind speed and  
228 direction, b: temperature and relative humidity) and aerosol properties (c: total  
229 surface and volume concentration, d and e: PNSD in the size range of 10 to 800 nm  
230 and particle number concentration in the range of 1.3 to 2.4 nm) during this field  
231 campaign. During our study, wind speed was typically quite low with an average of  
232  $1.18 \text{ m}\cdot\text{s}^{-1}$ , indicating stagnant meteorological conditions for the limited dilution of air  
233 pollutants at the current site. The temperature and relative humidity (RH) show  
234 opposite diurnal variation over the observational period, with the highest  
235 temperature and lowest RH during daytime and vice versa during nighttime. The  
236 observed time series of concentration of different trace gases during current study is  
237 shown in Fig. S1. To be specific, the campaign-averaged concentration of CO, O<sub>3</sub>, NO<sub>x</sub>  
238 and SO<sub>2</sub> was 1394 ppb, 7 ppb, 83 ppb and 10 ppb, respectively.

239 According to the PNSD and PSM data, five days, with four of which having  
240 significant burst of sub-3 nm clusters as shown in Fig.2e, were classified as NPF  
241 events out of the total experimental period. It has to be noted that on the day of  
242 November 18, though PSM data was not available due to technical issues, clear  
243 growth of nucleation mode particles with a typical banana-shape PNSD was observed,  
244 lasting for more than 12 hours. These particles under the growth of such a long time  
245 should not be from traffic emissions or transported. Therefore, it was also classified  
246 as an event day in our study. Considering all these five NPF event, this corresponds  
247 to an NPF frequency of 12.8%, which was lower than those at an urban site (i.e.,  
248 Beijing) in the same region during the same season Shen et al. (2018) (25.8%); Deng  
249 et al. (2020) (51.4%). Similar findings were also observed in Yue et al. (2009) and  
250 Wang et al. (2013), that NPF frequencies were higher at the Beijing urban site than at  
251 the corresponding regional background or rural site. Yue et al. (2009) and Wang et al.

252 (2013) attributed this to the higher pollution level and correspondingly higher  
 253 precursor content in the urban cities, leading to stronger NPF events there.

254 During our study, six days, with a slightly weak burst of sub-3 nm particles, were  
 255 identified as undefined days as their formation and growth rate cannot be calculated  
 256 accurately. For non-event days, we observed that during many of them some  
 257 nucleation-mode particles with size above 10 nm did appear. However, we did not  
 258 observe the burst of sub-3 nm clusters from the PSM measurements and moreover  
 259 no clear growth of these particles can be identified. This indicates that these small  
 260 particles probably are not from nucleation of  $\text{H}_2\text{SO}_4$  with other species and their  
 261 subsequent growth, but more likely local emissions (traffic exhausts) or long-range  
 262 transported.

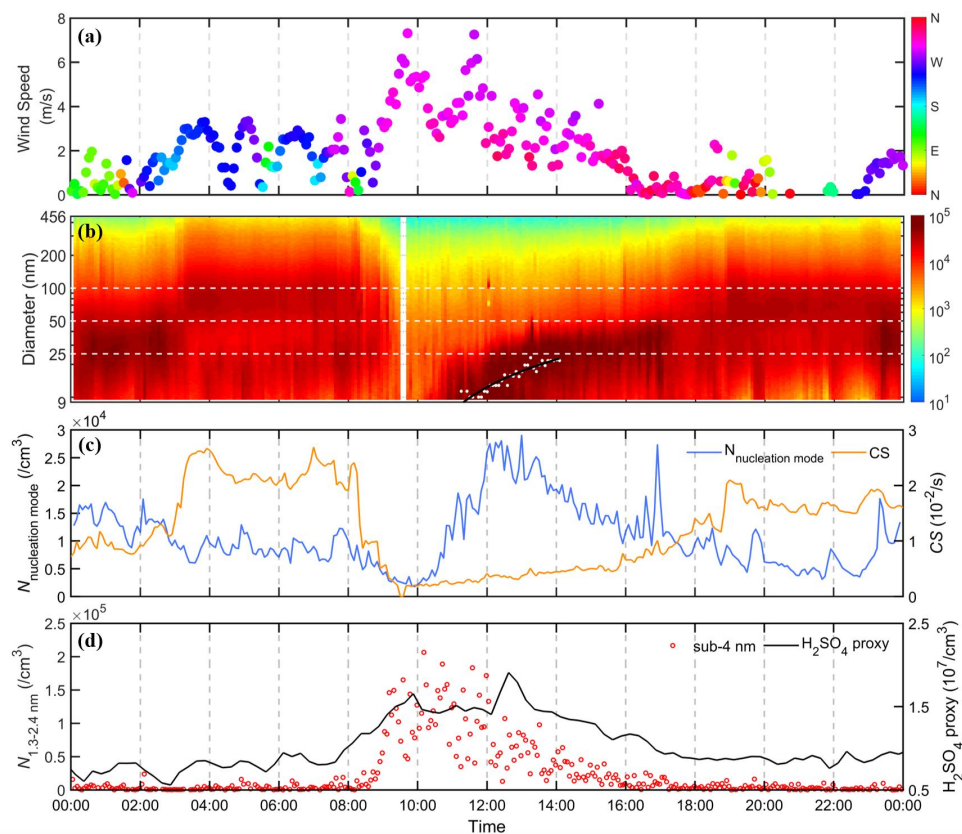


263  
 264 **Figure 2.** Time series of (a) wind speed and wind direction, (b) temperature, ( $T$ ) and relative  
 265 humidity (RH), (c) total particle surface and volume concentration calculated by using PNSD data,  
 266 (d) measured PNSD in the size range of 10 - 800 nm, (e) particle number concentration in the  
 267 range of 1.3 to 2.4 nm and  $\text{H}_2\text{SO}_4$  proxy concentration during the entire measurement period  
 268 (2018.11.12-2018.12.24). White portion indicates no data was available due to instrument  
 269 maintenance or power failure. Note that white portion in the PNSD in the size range of 10 - 15  
 270 nm, indicating no available data, is due to the technical problems of our SMPS system; therefore  
 271 data for that time period from a parallel SMPS covering sizes of 15 - 800 nm was used instead.

272

273 Figure 3 shows a typical NPF event on December 7 as an example. Northwest  
 274 wind prevailed with elevated wind speed starting from around 8:00 o'clock, which  
 275 was conducive to the diffusion of local pollutants, leading to a rapid decrease in CS

276 concurrently. At the same time, an obvious rise in  $\text{H}_2\text{SO}_4$  concentration was observed,  
 277 coinciding with a strong burst in the concentration of sub-3 nm clusters. Then, new  
 278 particles with diameter larger than 10 nm, as shown in Fig. 3b, gradually formed by  
 279 growth, exhibited as a visible banana shape in PNSD.



280 **Figure 3.** A case of NPF event on December 7 during this field campaign. Time series of (a) wind  
 281 speed and wind directions, (b) the PNSD in the size range of 10 - 450 nm (The white dotted line  
 282 represents the size with diameter at 25, 50, and 100 nm; black line represents the polynomial fit  
 283 of the measured PNSD, (c) the particle number concentration of nucleation mode (9 - 25nm) and  
 284 CS, (d) the number concentration of sub-3nm clusters and predicted concentration of sulfuric  
 285 acid.  
 286

287

288 For all the identified NPF events, the formation rate of 1.3 nm ( $J_{1.3}$ ) particles  
 289 ranged from  $6.0 \text{ cm}^{-3}\cdot\text{s}^{-1}$  to about  $30.4 \text{ cm}^{-3}\cdot\text{s}^{-1}$  with an average value of  $22.0 \text{ cm}^{-3}\cdot\text{s}^{-1}$   
 290 at our GC site during the measurement period. Note that most atmospheric  
 291 formation rates reported in China were based on the measured formation rates at  
 292 relatively larger size, i.e., 3-10 nm, which are so called the “apparent” particle  
 293 formation rates. In order to derive the formation rates of critical clusters from the  
 294 “apparent” particle formation rates (Kulmala et al., 2017), the nuclei GR or GR at

295 sub-3 nm is needed but usually remains unclear. Therefore, we focused more on the  
296 formation rate of particles at sizes below 3 nm in the following discussion. In  
297 principle, particle formation rate is inversely proportional to the CS, as the nucleation  
298 precursors or clusters would be scavenged more rapidly under higher CS conditions,  
299 leading to a slower nanoparticle formation with a lower  $J$ . However, as shown in  
300 Table 1, in spite of the higher CS, the particle formation rates at our site appear to be  
301 higher than those in clean environments. This kind of intensive NPF becomes more  
302 noticeable for those Chinese megacities, such as Shanghai, Beijing and Nanjing,  
303 having an even higher  $J$  and CS compared to that at our GC site. The most plausible  
304 explanation could be the higher abundance of nucleating precursors for NPF in those  
305 polluted atmospheres, which is indicated by the SA concentration, either measured  
306 in urban Shanghai and Nanjing or calculated in our study. To be specific, the mean SA  
307 proxy concentration during NPF at our GC site was around  $1.4 \cdot 10^7 \text{ cm}^{-3}$ , a factor of  
308 around 30 higher than that at Hyytiälä in Finland (Nieminen et al., 2014). The SA  
309 concentration during NPF at Shanghai (Xiao et al., 2015) and Nanjing (Herrmann et  
310 al., 2014) was even higher, being around  $4 \cdot 10^7 \text{ cm}^{-3}$ .

311

312

313

314 **Table 1.** Summaries of the parameters (average value) relevant for NPF event during wintertime in  
 315 China and other countries.

Station	Period	Frequency	$J$ ( $\text{cm}^{-3}\cdot\text{s}^{-1}$ )	$GR$ ( $\text{nm}\cdot\text{h}^{-1}$ )	$CS$ ( $10^{-2}\cdot\text{s}^{-1}$ )	$SA$ ( $10^6\cdot\text{cm}^{-3}$ )	Reference
GC <sup>R</sup>	2018.11.18	-	3.15 ( $J_{10}$ )	4.3	4.7	12.5	This study
GC <sup>R</sup>	2018.12.06	-	29.7 ( $J_{1.3}$ )	1.8	0.7	14.4	This study
GC <sup>R</sup>	2018.12.07	-	30.4 ( $J_{1.3}$ )	4.1	0.8	14.7	This study
GC <sup>R</sup>	2018.12.08	-	21.8 ( $J_{1.3}$ )	8.1	2.7	13.5	This study
GC <sup>R</sup>	2018.12.23	-	6.0 ( $J_{1.3}$ )	1.2	1.6	14.3	This study
GC <sup>R</sup> (mean)	2018.11.12-12.24	12.8%	22.0 ( $J_{1.3}$ )	3.9	2.1	13.9	This study
Thissio <sup>UB</sup>	2015.8-2016.8, 2017.2-2018.2 <sup>a</sup>	10.3%	1.55 ( $J_{10}$ )	3.48	0.79	6.33	(Kalkavouras et al., 2020)
New Delhi <sup>U</sup>	2002.10.26-2002.11.9	53.3%	7.3 ( $J_3$ )	14.9	5.75	-	(Mönkkönen et al., 2005)
Panyu <sup>U</sup>	Winter of 2011	21.3%	0.89 ( $J_{10}$ )	5.1	5.5	-	(Tan et al., 2016)
Shanghai <sup>U</sup>	2013.11.25-2014.1.25	21%	188 ( $J_{1.34}$ )	11.4	6.0	37	(Xiao et al., 2015)
Nanjing <sup>U</sup>	2011.11.18-2012.3.31	20%	33.2 ( $J_2$ )	8.5	2.4	45.3	(Herrmann et al., 2014)
Hongkong <sup>U</sup>	2010.10.25-2010.11.29	34.3%	2.94( $J_{5.5}$ )	3.86	0.8-6.2	9.17	(Guo et al., 2012)
Beijing <sup>U</sup>	2018.1.23-2018.3.31	51.5%	38 ( $J_{1.5}$ )	5.5	3.7	4.13	(Chu et al., 2021)
Ziyang <sup>R</sup>	2012.12.5-2013.1.5	23%	5.2( $J_3$ )	3.6	7.4	6.7	(Chen et al., 2014)
Melpitz <sup>R</sup>	Winter of 2003-2006	3%	0.7 ( $J_3$ )	5.6	1.2	0.123	(Hamed et al., 2010)
Melpitz <sup>R</sup>	Winter of 1996-1997	10%	4.9( $J_3$ )	4.1	0.9	0.259	(Hamed et al., 2010)
Pingyuan <sup>R</sup>	2017.11.3-2018.1.20	39.2%	164.2 ( $J_{1.6}$ )	3.9	1.9	2.45	(Fang et al., 2020)
Xinken <sup>R</sup>	2004.10.3-2004.11.5	25.9%	0.5-5.4( $J_3$ )	2.2.-19.8	-	-	(Liu et al., 2008)
Solapur <sup>R</sup>	2018.10-2019.2	28.9%	0.22-10.07( $J_{15}$ )	1.2-13.8	0.6-3	-	(Varghese et al., 2020)
Cyprus <sup>RB</sup>	2018.1-2018.2	69%	16.4( $J_{1.5}$ )	9.97	1.2	-	(Baalbaki et al., 2020)
SEAS <sup>O</sup>	Winter of 2018	5%	2.95( $J_{10}$ )	14.35	4.5	-	(Kompalli et al., 2020)
SMEAR II <sup>B</sup>	Winter of 1996-2003	24.2%	0.2-1.1( $J_3$ )	0.29-3.7	0.05-0.35	0.53	(Dal Maso et al., 2005)

316 SEAS: the southeastern Arabian Sea  
317 R: rural site UB: urban background site RB: rural background site U: urban site. B: background site O: ocean  
318 site  
319 a: only in wintertime -: no number



320 Although the formation rate of 1.3 nm particles is relatively high, the  
321 newly-formed particles at our GC site usually cannot grow into very large particles  
322 within a short time, indicative by their low GR. The average value of  $GR_{1.3-2.4}$  and  
323  $GR_{9-15}$  at our site was  $0.5 \text{ nm}\cdot\text{h}^{-1}$  and  $3.9 \text{ nm}\cdot\text{h}^{-1}$ , respectively, being generally lower  
324 than many clean environments ( $GR_{1-3}$  of  $0.9 \text{ nm}\cdot\text{h}^{-1}$  for Hyytiälä (Kulmala, 2013), of  
325  $5.1 \text{ nm}\cdot\text{h}^{-1}$  for Jungfrauoch (Boulon et al., 2010)), but similar to those at urban  
326 Beijing (Chu et al., 2021) and rural Pingyuan (Fang et al., 2020). This could be  
327 attributed by the high CS or CoagS at those polluted environments as the growth of  
328 small particles is limited, which are more vulnerable to the coagulation scavenging.  
329 However, despite the high CoagS, the observed GR at Shanghai and Nanjing was still  
330 exceptionally high. This discrepancy suggests that besides the high concentration of  
331 precursors, mainly  $\text{H}_2\text{SO}_4$ , in polluted environments including both rural and urban  
332 sites, other precursors with different efficiency for nanoparticle growth, and other  
333 involving mechanisms, for instance, multiphase reactions, may all contribute to the  
334 nanoparticle growth, yet to be elucidated.

### 335 **3.2. Potential mechanisms for NPF events in the rural NCP**

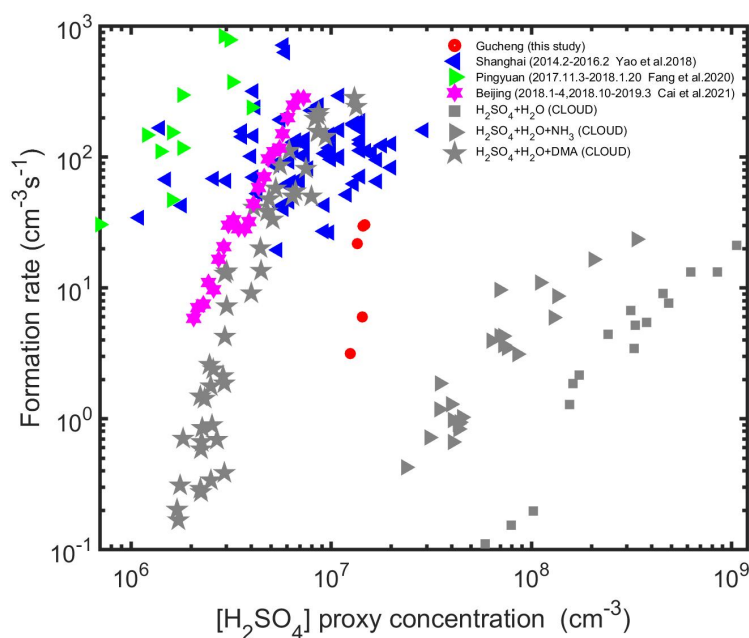
336 To further understand the dominating nucleation mechanism in the rural  
337 atmosphere of NCP in China, we plotted the measured formation rate of 1.3 nm  
338 particles ( $J_{1.3}$ ) against the simulated  $\text{H}_2\text{SO}_4$  concentration and compared the results  
339 to previous studies conducted in different environments, as shown in Fig. 4. As  
340 illustrated by the significant correlation between the concentration of sulfuric acid  
341 and the particle formation rates, sulfuric acid is considered to be the driving species  
342 in the initial steps of NPF as confirmed conventionally. However, the obtained  
343  $J_{1.3}$ - $\text{H}_2\text{SO}_4$  relationship for current environment appeared to deviate largely from  
344 those obtained by other studies. If only referring to the slope of the  $J_{1.3}$ - $\text{H}_2\text{SO}_4$   
345 relationship, our results seem to approximate most to the ones measured by these  
346 CLOUD (The Cosmics Leaving OUtdoor Droplets chamber) experiments based on the  
347 mechanism of  $\text{H}_2\text{SO}_4$ -DMA nucleation. However, without the direct measurements of

348 other potential precursors, the molecules stabilizing H<sub>2</sub>SO<sub>4</sub> clustering still remain  
349 unclear.

350 Comparing the particle formation rates reported in different environments in  
351 China, our results were of the similar magnitude as that in Beijing (Cai et al., 2021b),  
352 an urban site in the NCP. It has to be noted that their study was conducted during a  
353 much longer time and completely covered the measurement period of our study.  
354 More importantly, during the five days of events in our study, NPF concurrently  
355 occurred at their measurement site (Liu et al., 2020). Additionally, for these five  
356 event days air masses arriving at our site followed similar transport paths to that at  
357 urban Beijing (see Fig. S2 as an example in the supplement), both originating from  
358 Siberia areas, where concentration of gaseous pollutants and particulate matter was  
359 typically quite low, through the northwest of the observational sites. Taking both  
360 evidence, we hypothesis that NPF events during these days in this area might be a  
361 regional phenomenon, sharing the same or similar nucleation mechanism. Cai et al.  
362 (2021) and Yan et al. (2021) further concluded that H<sub>2</sub>SO<sub>4</sub>-DMA was the dominating  
363 nucleation mechanism for urban Beijing with an additional support from the  
364 measured C2-amine concentration. Considering the similarities between these two  
365 sites, we speculated that the clustering of H<sub>2</sub>SO<sub>4</sub> with DMA may also dominate the  
366 nucleation process at our site during winter, though future work is needed to verify  
367 current hypothesis.

368 On the other hand, we noticed that our results deviate significantly from the  
369 measured formation rate at Pingyuan (Fang et al., 2020), another rural site in the NCP.  
370 They concluded that neither H<sub>2</sub>SO<sub>4</sub>-NH<sub>3</sub> nor H<sub>2</sub>SO<sub>4</sub>-DMA mechanisms could fully  
371 explain their observed particle formation rate but suggested that gaseous  
372 dicarboxylic acids were the dominating species for the initial step of H<sub>2</sub>SO<sub>4</sub> clustering  
373 under diacid-rich environment. Being likewise the rural environment of NCP, we  
374 cannot completely rule out the contribution of dicarboxylic acids to the H<sub>2</sub>SO<sub>4</sub>  
375 stabilizing. However, as illustrated in Fig. S4, the concentration of these four  
376 dicarboxylic acids during NPF events were in general lower than that during  
377 non-event days. Furthermore, during the daytime of events days when NPF was

378 typically initiated, the signals of these diacids obtained from the I-CIMS did not show  
 379 clear increase, unlike sulfuric acid, but rather elevated during the night time (see Fig.  
 380 S5), being obviously different from the case of Pingyuan. Hence, the involvements of  
 381 diacids during the initial steps of nucleation under current rural atmosphere might  
 382 not hold. This statement does not necessarily mean that our previous inference was  
 383 incorrect, but on the other hand, provides some hints that though NPF events in the  
 384 NCP is regional, there might be no uniform theory but multiple mechanisms  
 385 coexisting to explain its feature with the dominating one varying upon different  
 386 emission patterns or meteorological conditions.



387  
 388 **Figure 4.** The particle formation rate ( $J_{1,3}$ ) as a function of  $H_2SO_4$  concentration for our study as  
 389 well as for urban Shanghai (Yao et al., 2018), Beijing (Cai et al., 2021b), rural Pingyuan (Fang et al.,  
 390 2020) and CLOUD measurements. Gray square, triangle, pentagram, and diamond represents the  
 391 CLOUD data for  $H_2SO_4+H_2O$ ,  $H_2SO_4+H_2O+NH_3$ ,  $H_2SO_4+H_2O+DMA$  (Kirkby et al. (2011) and  
 392 Riccobono et al. (2014)), where DMA represents dimethylamine.

393

### 394 3.3 Governing factors for the occurrence of NPF in rural NCP

395

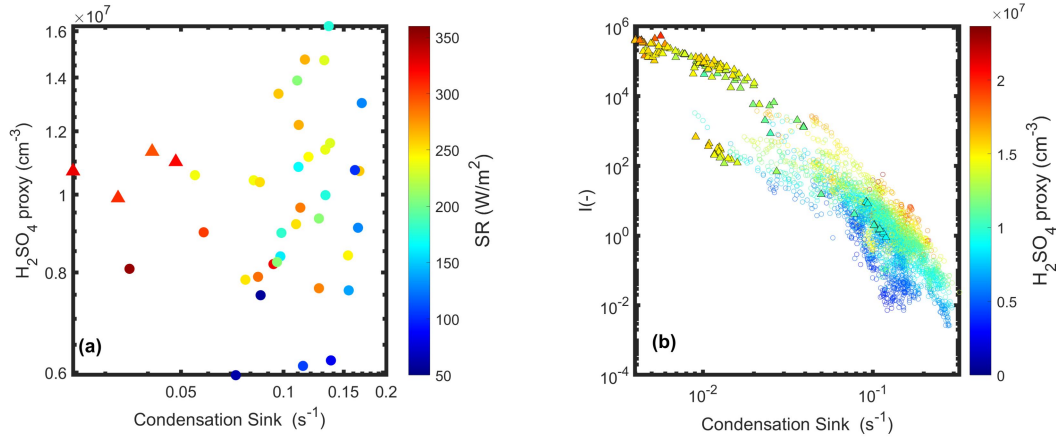
396 The high concentration of  $SO_2$ ,  $NH_3$ ,  $NO_x$ , VOCs (Chu et al., 2019) as well as fine  
 397 particles makes the NCP of China an unique condition for NPF compared to many  
 398 other environments. In principle, the competition between how fast the

399 newly-formed clusters grow and how fast they are scavenged determines whether  
400 NPF will occur or not in the atmosphere. However, in the NCP, the concentration of  
401 SA was typically quite high, probably reaching its maximum rate to form clusters.  
402 Thus, CS or CoagS becomes the dominant factor controlling the occurrence of NPF.  
403 This was partly confirmed by existing observations, for instance, Cai et al. (2021)  
404 found that H<sub>2</sub>SO<sub>4</sub> was high enough in urban Beijing, but not necessarily led to the  
405 occurrence of NPF there. They pointed out that as long as CS or CoagS was below a  
406 certain threshold (Cai et al., 2017), NPF is very likely take place.

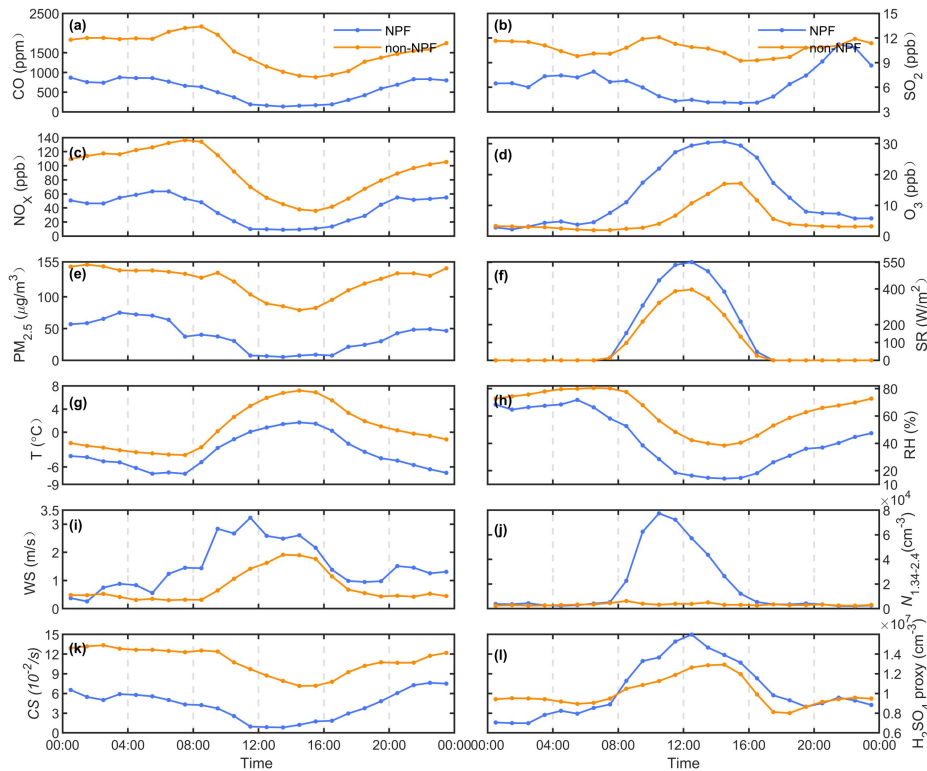
407 Was this also true for rural atmosphere in the NCP? By comparing with  
408 non-event days at our site (see Fig. 5a), we noticed that H<sub>2</sub>SO<sub>4</sub> level was not  
409 significantly higher but sometimes even lower than that during non-event days. In  
410 other words, the abundance of H<sub>2</sub>SO<sub>4</sub> did not always lead to NPF; and it was only  
411 when CS was significantly lowered that the event became more likely to occur. This  
412 strongly demonstrates the similarity between our site with urban Beijing, that CS  
413 would be the limiting factor for the occurrence of NPF. However, we noticed that  
414 there were a very few cases (two cases) that CS was somewhat quite low, being  
415 quite close to that under those event days, yet NPF still did not occur. The most  
416 plausible explanation for this could be on the one hand the lowered H<sub>2</sub>SO<sub>4</sub>  
417 concentration at these days (as shown in Fig. 5a) and on the other hand the other  
418 nucleating species rather than H<sub>2</sub>SO<sub>4</sub> may not be always enough to initiate  
419 nucleation at this site.

420 As previously stated that the dimensionless criterion, *I*, is a good quantitative  
421 indicator to predict whether an NPF occurs or not during a certain day, we plotted *I*  
422 against the condensational sink for NPF days and other days under different H<sub>2</sub>SO<sub>4</sub>  
423 level. Cai et al. (2021) found that the larger the *I* value, the higher frequency that  
424 NPF events occurred for both urban Beijing and Shanghai, which was also clearly  
425 revealed by our results. On the one hand, as shown in Fig. 5b, the largest *I* values  
426 were mostly observed for NPF days, confirming its feasibility in predicting the  
427 occurrence of NPF events. On the other hand, the obtained *I* anti-correlated with CS  
428 quite well, while the influence from the available H<sub>2</sub>SO<sub>4</sub> was not obvious. This

429 strongly suggests that CS was the dominating factor governing the appearance of  
 430 NPF events at current environment, being highly consistent with the feature in  
 431 Beijing.



432  
 433 **Figure 5.** (a)  $H_2SO_4$  concentration as a function of condensation sink during both event days and  
 434 non-event days during our study. (b) The dimensionless indicator,  $I$ , as a function of the  
 435 condensational sink. For both panels, the triangles indicate data for event days while the circles  
 436 indicate data for non-event days. The colorbar indicates: solar radiation (left panel) and  $H_2SO_4$   
 437 proxy concentration (right panel).



438  
 439 **Figure 6.** Diurnal variation of (a) CO, (b)  $SO_2$ , (c)  $NO_x$ , (d)  $O_3$ , (e)  $PM_{2.5}$ , (f) Solar radiation (SR), (g)  $T$ ,  
 440 (h) RH, (i) wind speed (WS), (j) number concentration of sub-3nm cluster, (k) CS, and (l)  $H_2SO_4$   
 441 proxy during the NPF and non-NPF days during this field campaign. These values were  
 442 averaged over the five NPF days and 28 non-event days, respectively.

443 On the other hand, we found that RH level under event days was generally  
444 lower than that on non-event days (see Fig. 6). This is similar to the cases that NPF  
445 was observed in Beijing by Yue et al. (2009), who suggested that photochemical  
446 reactions were faster on sunny days with low RH. In addition to this, ambient  
447 temperature during NPF was relatively lower than that on non-event days (Kirkby et  
448 al. (2011); Riccobono et al. (2014)). Yan et al. (2021) considered that temperature can  
449 affect the stability of H<sub>2</sub>SO<sub>4</sub> clustering and thus influence NPF. Therefore, all these  
450 factors could be the potential reasons increase or decrease the probability of NPF to  
451 occur in current rural areas. It has to be noted that all these features, including  
452 reduced RH level as well as ambient *T* during event days, could be coincidence with  
453 reduced CS over clean days, for instance, being a consequence of air masses  
454 originating from the north and bringing dryer, colder and cleaner air to the site.  
455 Therefore, current discussion in this regard becomes ambiguous and may be inclusive,  
456 but should still be considered separately when larger datasets are available.  
457 Moreover, we observed that O<sub>3</sub> concentration was clearly higher during event days,  
458 implying that other condensable vapors, for instance, organics, that involve O<sub>3</sub>,  
459 among others, in forming HOM, might also be important to NPF in this region.  
460 Although these organic compounds formed through O<sub>3</sub> oxidation (Mohr et al., 2019)  
461 may not necessarily participate in H<sub>2</sub>SO<sub>4</sub> clustering, they may considerably contribute  
462 to the growth of newly-formed particles, which should not be ruled out in the study  
463 of NPF for this region and also need to be investigated in the future.

464

#### 465 4. Summary and conclusions

466

467 Most previous studies dealing with NPF in China were mainly based on  
468 measurements of particles at larger sizes, typically above 3 nm, whereas detection of  
469 particles at sub-3 nm range was quite limited. In our study, by coupling a PSM with a  
470 traditional SMPS, We were able to measure the particle number size distribution  
471 down to 1.3 nm during NPF events in the wintertime at a rural site of the NCP.  
472 Correspondingly, formation rate of particles at 1.3 nm was obtained, widening the

473 data pool concerning the feature of NPF for this region. At current rural environment,  
474 high level of  $\text{H}_2\text{SO}_4$  may not always initiate the occurrence of NPF. Only at the  
475 condition that the CS was considerably low, NPF events were more likely to take place.  
476 This feature is quite similar to that of the urban atmosphere of NCP, whereas NPF  
477 events were usually characterized with high formation rates, high CS and high  $\text{H}_2\text{SO}_4$   
478 concentration. However, as our  $\text{H}_2\text{SO}_4$  concentration was predicted from empirical  
479 parameters, particular cautions regarding their associated uncertainties should be  
480 considered. Yang et al. (2021) demonstrated that the derived fitting parameters for  
481 the calculations of  $\text{H}_2\text{SO}_4$  proxy may vary from site to site and between different  
482 seasons. For instance, they considered the products from the ozonolysis of alkenes  
483 were able to oxidize  $\text{SO}_2$  to form gaseous  $\text{H}_2\text{SO}_4$ . Moreover, they pointed out that  
484  $\text{H}_2\text{SO}_4$  could be from primary emissions, such as vehicles or freshly emitted plumes.  
485 Sulfuric acid from these sources could account for 10% of the total  $\text{H}_2\text{SO}_4$  in the  
486 atmosphere. These aspects were not comprehensively considered in our calculations,  
487 which could bring huge uncertainties or errors to the estimation. Thereby, direct  
488 measurements for the  $\text{H}_2\text{SO}_4$  concentration should be implemented in the future  
489 before driving any further conclusion.

490

491

492

493

494

495

496

497

498

499

500

501

502

503 **Declaration of interest statement.**

504 The authors declare that they have no known competing financial interests or  
505 personal relationships that could have appeared to influence the work reported in  
506 this paper.

507

508 **Data availability.**

509 The details data can be obtained from <https://doi.org/10.5281/zenodo.7326388>  
510 (Hong, 2022).

511

512 **Author contributions.**

513 JH collected the resources, wrote and finalized the manuscript, MT analyzed the data,  
514 plotted the figures and wrote the original draft, QQW and NM planned the study,  
515 collected the resources, reviewed the manuscript. SWZ, SBZ, XHP, LHX, GL, UK  
516 conducted the measurements, CY, JCT, YK, YH, YQZ, WYX, GSZ, BY, ZBW discussed the  
517 results. YFC and HS contributed to fund acquisition.

518

519 **Competing interests.**

520 Hang Su and Yafang Cheng are members of the editorial board of Atmospheric  
521 Chemistry and Physics

522

523 **Acknowledgements.**

524 This work is supported by the National Natural Science Foundation of China (grant no.  
525 42175117, 41907182, 41877303, 91644218) and the National key R&D Program of  
526 China (2018YFC0213901), the Fundamental Research Funds for the Central  
527 Universities (21621105), the Guangdong Innovative and Entrepreneurial Research  
528 Team Program (Research team on atmospheric environmental roles and effects of  
529 carbonaceous species: 2016ZT06N263), and Special Fund Project for Science and  
530 Technology Innovation Strategy of Guangdong Province (2019B121205004).



## 531 References

- 532 Almeida, J., Schobesberger, S., Kürten, A., Ortega, I. K., Kupiainen-Määttä, O., Praplan, A. P.,  
533 Adamov, A., Amorim, A., Bianchi, F., Breitenlechner, M., David, A., Dommen, J., Donahue, N. M.,  
534 Downard, A., Dunne, E., Duplissy, J., Ehrhart, S., Flagan, R. C., Franchin, A., Guida, R., Hakala, J.,  
535 Hansel, A., Heinritzi, M., Henschel, H., Jokinen, T., Junninen, H., Kajos, M., Kangasluoma, J.,  
536 Keskinen, H., Kupc, A., Kurtén, T., Kvashin, A. N., Laaksonen, A., Lehtipalo, K., Leiminger, M.,  
537 Leppä, J., Loukonen, V., Makhmutov, V., Mathot, S., McGrath, M. J., Nieminen, T., Olenius, T.,  
538 Onnela, A., Petäjä, T., Riccobono, F., Riipinen, I., Rissanen, M., Rondo, L., Ruuskanen, T., Santos, F.  
539 D., Sarnela, N., Schallhart, S., Schnitzhofer, R., Seinfeld, J. H., Simon, M., Sipilä, M., Stozhkov, Y.,  
540 Stratmann, F., Tomé, A., Tröstl, J., Tsagkogeorgas, G., Vaattovaara, P., Viisanen, Y., Virtanen, A.,  
541 Vrtala, A., Wagner, P. E., Weingartner, E., Wex, H., Williamson, C., Wimmer, D., Ye, P., Yli-Juuti, T.,  
542 Carslaw, K. S., Kulmala, M., Curtius, J., Baltensperger, U., Worsnop, D. R., Vehkamäki, H., and  
543 Kirkby, J.: Molecular understanding of sulphuric acid-amine particle nucleation in the atmosphere,  
544 *Nature*, 502, 359–363, <https://doi.org/10.1038/nature12663>, 2013.
- 545 Baalbaki, R., Pikridas, M., Jokinen, T., Laurila, T., Dada, L., Bezantakos, S., Ahonen, L., Neitola, K.,  
546 Maisser, A., Bimenyimana, E., Christodoulou, A., Unga, F., Savvides, C., Lehtipalo, K.,  
547 Kangasluoma, J., Biskos, G., Petäjä, T., Kerminen, V.-M., Sciare, J., and Kulmala, M.: Towards  
548 understanding the mechanisms of new particle formation in the Eastern Mediterranean, *Atmos.*  
549 *Chem. Phys. Discuss.*, 1–44, <https://doi.org/10.5194/acp-2020-1066>, 2020.
- 550 Berndt, T., Stratmann, F., Sipilä, M., Vanhanen, J., Petäjä, T., Mikkilä, J., Grüner, A., Spindler, G.,  
551 Lee Mauldin, R., Curtius, J., Kulmala, M., and Heintzenberg, J.: Laboratory study on new particle  
552 formation from the reaction OH + SO<sub>2</sub>: Influence of experimental conditions, H<sub>2</sub>O vapour, NH<sub>3</sub>  
553 and the amine tert-butylamine on the overall process, *Atmos. Chem. Phys.*, 10, 7101–7116,  
554 <https://doi.org/10.5194/acp-10-7101-2010>, 2010.
- 555 Bianchi, F., Tröstl, J., Junninen, H., Frege, C., Henne, S., Hoyle, C. R., Molteni, U., Herrmann, E.,  
556 Adamov, A., Bukowiecki, N., Chen, X., Duplissy, J., Gysel, M., Hutterli, M., Kangasluoma, J.,  
557 Kontkanen, J., Kürten, A., Manninen, H. E., Münch, S., Peräkylä, O., Petäjä, T., Rondo, L.,  
558 Williamson, C., Weingartner, E., Curtius, J., Worsnop, D. R., Kulmala, M., Dommen, J., and  
559 Baltensperger, U.: New particle formation in the free troposphere: A question of chemistry and  
560 timing, *Science (80- )*, 352, 1109–1112, <https://doi.org/10.1126/science.aad5456>, 2016.
- 561 Boulon, J., Sellegri, K., Venzac, H., Picard, D., Weingartner, E., Wehrle, G., Collaud Coen, M.,  
562 Bütikofer, R., Flückiger, E., Baltensperger, U., and Laj, P.: New particle formation and ultrafine  
563 charged aerosol climatology at a high altitude site in the Alps (Jungfrauoch, 3580 m a.s.l.,  
564 Switzerland), *Atmos. Chem. Phys.*, 10, 9333–9349, <https://doi.org/10.5194/acp-10-9333-2010>,  
565 2010.
- 566 Cai, R. and Jiang, J.: A new balance formula to estimate new particle formation rate: Reevaluating  
567 the effect of coagulation scavenging, *Atmos. Chem. Phys.*, 17, 12659–12675,  
568 <https://doi.org/10.5194/acp-17-12659-2017>, 2017.
- 569 Cai, R., Yang, D., Fu, Y., Wang, X., Li, X., Ma, Y., Hao, J., Zheng, J., and Jiang, J.: Aerosol surface  
570 area concentration: A governing factor in new particle formation in Beijing, *Atmos. Chem. Phys.*,  
571 17, 12327–12340, <https://doi.org/10.5194/acp-17-12327-2017>, 2017.

572 Cai, R., Yan, C., Worsnop, D. R., Bianchi, F., Kerminen, V.-M., Liu, Y., Wang, L., Zheng, J., Kulmala,  
573 M., and Jiang, J.: An indicator for sulfuric acid–amine nucleation in atmospheric environments,  
574 *Aerosol Sci. Technol.*, 55, 1059–1069, <https://doi.org/10.1080/02786826.2021.1922598>, 2021a.

575 Cai, R., Yan, C., Yang, D., Yin, R., Lu, Y., Deng, C., Fu, Y., Ruan, J., Li, X., Kontkanen, J., Zhang, Q.,  
576 Kangasluoma, J., Ma, Y., Hao, J., Worsnop, D. R., Bianchi, F., Paasonen, P., Kerminen, V. M., Liu, Y.,  
577 Wang, L., Zheng, J., Kulmala, M., and Jiang, J.: Sulfuric acid-amine nucleation in urban Beijing,  
578 *Atmos. Chem. Phys.*, 21, 2457–2468, <https://doi.org/10.5194/acp-21-2457-2021>, 2021b.

579 CHEN Chen, HU Min, WU Zhi-jun, WU Yu-sheng, GUO Song, CHEN Wen-tai, LUO Bin, SHAO Min,  
580 ZHANG Yuan-hang, X. S.: Characterization of new particle formation event in the rural site of  
581 Sichuan Basin and its contribution to cloud condensation nuclei., *China Environ. Sci.*, 34,  
582 2764–2772, 2014.

583 Chu, B., Matti Kerminen, V., Bianchi, F., Yan, C., Petäjä, T., and Kulmala, M.: Atmospheric new  
584 particle formation in China, *Atmos. Chem. Phys.*, 19, 115–138,  
585 <https://doi.org/10.5194/acp-19-115-2019>, 2019.

586 Chu, B., Dada, L., Liu, Y., Yao, L., Wang, Y., Du, W., Cai, J., Dällenbach, K. R., Chen, X., Simonen, P.,  
587 Zhou, Y., Deng, C., Fu, Y., Yin, R., Li, H., He, X. C., Feng, Z., Yan, C., Kangasluoma, J., Bianchi, F.,  
588 Jiang, J., Kujansuu, J., Kerminen, V. M., Petäjä, T., He, H., and Kulmala, M.: Particle growth with  
589 photochemical age from new particle formation to haze in the winter of Beijing, China, *Sci. Total*  
590 *Environ.*, 753, 142207, <https://doi.org/10.1016/j.scitotenv.2020.142207>, 2021.

591 Dal Maso, M., Kulmala, M., Riipinen, I., Wagner, R., Hussein, T., Aalto, P. P., and Lehtinen, K. E. J.:  
592 Formation and growth of fresh atmospheric aerosols: Eight years of aerosol size distribution data  
593 from SMEAR II, Hyytiälä, Finland, *Boreal Environ. Res.*, 10, 323–336, 2005.

594 Deng, C., Fu, Y., Dada, L., Yan, C., Cai, R., Yang, D., Zhou, Y., Yin, R., Lu, Y., Li, X., Qiao, X., Fan, X.,  
595 Nie, W., Kontkanen, J., Kangasluoma, J., Chu, B., Ding, A., Kerminen, V.-M., Paasonen, P.,  
596 Worsnop, D. R., Bianchi, F., Liu, Y., Zheng, J., Wang, L., Kulmala, M., and Jiang, J.: Seasonal  
597 Characteristics of New Particle Formation and Growth in Urban Beijing, *Environ. Sci. Technol.*,  
598 [acs.est.0c00808](https://doi.org/10.1021/acs.est.0c00808), <https://doi.org/10.1021/acs.est.0c00808>, 2020.

599 Dunne, E. M., Gordon, H., Kürten, A., Almeida, J., Duplissy, J., Williamson, C., Ortega, I. K., Pringle,  
600 K. J., Adamov, A., Baltensperger, U., Barmet, P., Benduhn, F., Bianchi, F., Breitenlechner, M.,  
601 Clarke, A., Curtius, J., Dommen, J., Donahue, N. M., Ehrhart, S., Flagan, R. C., Franchin, A., Guida,  
602 R., Hakala, J., Hansel, A., Heinritzi, M., Jokinen, T., Kangasluoma, J., Kirkby, J., Kulmala, M., Kupc,  
603 A., Lawler, M. J., Lehtipalo, K., Makhmutov, V., Mann, G., Mathot, S., Merikanto, J., Miettinen, P.,  
604 Nenes, A., Onnela, A., Rap, A., Reddington, C. L. S., Riccobono, F., Richards, N. A. D., Rissanen, M.  
605 P., Rondo, L., Sarnela, N., Schobesberger, S., Sengupta, K., Simon, M., Sipilä, M., Smith, J. N.,  
606 Stozkhov, Y., Tomé, A., Tröstl, J., Wagner, P. E., Wimmer, D., Winkler, P. M., Worsnop, D. R., and  
607 Carslaw, K. S.: Global atmospheric particle formation from CERN CLOUD measurements, *Science*  
608 (80- ), 354, 1119–1124, <https://doi.org/10.1126/science.aaf2649>, 2016.

609 Ehn, M., Thornton, J. A., Kleist, E., Sipilä, M., Junninen, H., Pullinen, I., Springer, M., Rubach, F.,  
610 Tillmann, R., Lee, B., Lopez-Hilfiker, F., Andres, S., Acir, I.-H., Rissanen, M., Jokinen, T.,  
611 Schobesberger, S., Kangasluoma, J., Kontkanen, J., Nieminen, T., Kurtén, T., Nielsen, L. B.,  
612 Jørgensen, S., Kjaergaard, H. G., Canagaratna, M., Maso, M. D., Berndt, T., Petäjä, T., Wahner, A.,  
613 Kerminen, V.-M., Kulmala, M., Worsnop, D. R., Wildt, J., and Mentel, T. F.: A large source of  
614 low-volatility secondary organic aerosol., *Nature*, 506, 476–9,  
615 <https://doi.org/10.1038/nature13032>, 2014.

616 Fang, X., Hu, M., Shang, D., Tang, R., Shi, L., Olenius, T., Wang, Y., Wang, H., Zhang, Z., Chen, S.,  
617 Yu, X., Zhu, W., Lou, S., Ma, Y., Li, X., Zeng, L., Wu, Z., Zheng, J., and Guo, S.: Observational  
618 Evidence for the Involvement of Dicarboxylic Acids in Particle Nucleation, *Environ. Sci. Technol.*  
619 *Lett.*, <https://doi.org/10.1021/acs.estlett.0c00270>, 2020.

620 Guo, H., Wang, D. W., Cheung, K., Ling, Z. H., Chan, C. K., and Yao, X. H.: Observation of aerosol  
621 size distribution and new particle formation at a mountain site in subtropical Hong Kong, *Atmos.*  
622 *Chem. Phys.*, **12**, 9923–9939, <https://doi.org/10.5194/acp-12-9923-2012>, 2012.

623 Guo, S., Hu, M., Zamora, M. L., Peng, J., Shang, D., Zheng, J., Du, Z., Wu, Z., Shao, M., Zeng, L.,  
624 Molina, M. J., and Zhang, R.: Elucidating severe urban haze formation in China, *Proc. Natl. Acad.*  
625 *Sci. U. S. A.*, **111**, 17373–17378, <https://doi.org/10.1073/pnas.1419604111>, 2014.

626 Hamed, A., Birmili, W., Joutsensaari, J., Mikkonen, S., Asmi, A., Wehner, B., Spindler, G., Jaatinen,  
627 A., Wiedensohler, A., Korhonen, H., J. Lehtinen, K. E., and Laaksonen, A.: Changes in the  
628 production rate of secondary aerosol particles in Central Europe in view of decreasing SO<sub>2</sub>  
629 emissions between 1996 and 2006, *Atmos. Chem. Phys.*, **10**, 1071–1091,  
630 <https://doi.org/10.5194/acp-10-1071-2010>, 2010.

631 Herrmann, E., Ding, A. J., Kerminen, V. M., Petäjä, T., Yang, X. Q., Sun, J. N., Qi, X. M., Manninen,  
632 H., Hakala, J., Nieminen, T., Aalto, P. P., Kulmala, M., and Fu, C. B.: Aerosols and nucleation in  
633 eastern China: First insights from the new SORPES-NJU station, *Atmos. Chem. Phys.*, **14**,  
634 2169–2183, <https://doi.org/10.5194/acp-14-2169-2014>, 2014.

635 Hussein, T., Dal Maso, M., Petäjä, T., Koponen, I. K., Paatero, P., Aalto, P. P., Hämeri, K., and  
636 Kulmala, M.: Evaluation of an automatic algorithm for fitting the particle number size  
637 distributions, *Boreal Environ. Res.*, **10**, 337–355, 2005.

638 Jokinen, T., Sipilä, M., Junninen, H., Ehn, M., Lönn, G., Hakala, J., Petäjä, T., Mauldin, R. L.,  
639 Kulmala, M., and Worsnop, D. R.: Atmospheric sulphuric acid and neutral cluster measurements  
640 using CI-API-TOF, *Atmos. Chem. Phys.*, **12**, 4117–4125,  
641 <https://doi.org/10.5194/acp-12-4117-2012>, 2012.

642 Kalkavouras, P., Bougiatioti, A., Grivas, G., Stavroulas, I., Kalivitis, N., Liakakou, E., Gerasopoulos,  
643 E., Pilinis, C., and Mihalopoulos, N.: On the regional aspects of new particle formation in the  
644 Eastern Mediterranean: A comparative study between a background and an urban site based on  
645 long term observations, *Atmos. Res.*, **239**, 104911,  
646 <https://doi.org/10.1016/j.atmosres.2020.104911>, 2020.

647 Kirkby, J., Curtius, J., Almeida, J., Dunne, E., Duplissy, J., Ehrhart, S., Franchin, A., Gagné, S., Ickes,  
648 L., Kürten, A., Kupc, A., Metzger, A., Riccobono, F., Rondo, L., Schobesberger, S., Tsagkogeorgas,  
649 G., Wimmer, D., Amorim, A., Bianchi, F., Breitenlechner, M., David, A., Dommen, J., Downard, A.,  
650 Ehn, M., Flagan, R. C., Haider, S., Hansel, A., Hauser, D., Jud, W., Junninen, H., Kreissl, F., Kvashin,  
651 A., Laaksonen, A., Lehtipalo, K., Lima, J., Lovejoy, E. R., Makhmutov, V., Mathot, S., Mikkilä, J.,  
652 Minginette, P., Mogo, S., Nieminen, T., Onnela, A., Pereira, P., Petäjä, T., Schnitzhofer, R.,  
653 Seinfeld, J. H., Sipilä, M., Stozhkov, Y., Stratmann, F., Tomé, A., Vanhanen, J., Viisanen, Y., Vrtala,  
654 A., Wagner, P. E., Walther, H., Weingartner, E., Wex, H., Winkler, P. M., Carslaw, K. S., Worsnop,  
655 D. R., Baltensperger, U., and Kulmala, M.: Role of sulphuric acid, ammonia and galactic cosmic  
656 rays in atmospheric aerosol nucleation, *Nature*, **476**, 429–435,  
657 <https://doi.org/10.1038/nature10343>, 2011.

658 Kirkby, J., Duplissy, J., Sengupta, K., Frege, C., Gordon, H., Williamson, C., Heinritzi, M., Simon, M.,  
659 Yan, C., Almeida, J., Trostl, J., Nieminen, T., Ortega, I. K., Wagner, R., Adamov, A., Amorim, A.,

660 Bernhammer, A. K., Bianchi, F., Breitenlechner, M., Brilke, S., Chen, X., Craven, J., Dias, A., Ehrhart,  
661 S., Flagan, R. C., Franchin, A., Fuchs, C., Guida, R., Hakala, J., Hoyle, C. R., Jokinen, T., Junninen, H.,  
662 Kangasluoma, J., Kim, J., Krapf, M., Kurten, A., Laaksonen, A., Lehtipalo, K., Makhmutov, V.,  
663 Mathot, S., Molteni, U., Onnela, A., Perakyla, O., Piel, F., Petaja, T., Praplan, A. P., Pringle, K., Rap,  
664 A., Richards, N. A. D., Riipinen, I., Rissanen, M. P., Rondo, L., Sarnela, N., Schobesberger, S., Scott,  
665 C. E., Seinfeld, J. H., Sipila, M., Steiner, G., Stozhkov, Y., Stratmann, F., Tomé, A., Virtanen, A.,  
666 Vogel, A. L., Wagner, A. C., Wagner, P. E., Weingartner, E., Wimmer, D., Winkler, P. M., Ye, P.,  
667 Zhang, X., Hansel, A., Dommen, J., Donahue, N. M., Worsnop, D. R., Baltensperger, U., Kulmala,  
668 M., Carslaw, K. S., and Curtius, J.: Ion-induced nucleation of pure biogenic particles, *Nature*, 533,  
669 521–526, <https://doi.org/10.1038/nature17953>, 2016.

670 Kompalli, S. K., Nair, V. S., Jayachandran, V., Gogoi, M. M., and Babu, S. S.: Particle number size  
671 distributions and new particle formation events over the northern Indian Ocean during  
672 continental outflow, *Atmos. Environ.*, 238, 117719,  
673 <https://doi.org/10.1016/j.atmosenv.2020.117719>, 2020.

674 Kuang, C., Riipinen, I., Sihto, S.-L., Kulmala, M., McCormick, A. V., and McMurry, P. H.: An  
675 improved criterion for new particle formation in diverse atmospheric environments, *Atmos.*  
676 *Chem. Phys.*, 10, 8469–8480, <https://doi.org/10.5194/acp-10-8469-2010>, 2010.

677 Kulmala, M.: Direct Observations of Atmospheric Aerosol Nucleation, *Science* (80-. ), 943,  
678 <https://doi.org/10.1126/science.1227385>, 2013.

679 Kulmala, M., Pirjola, L., and Mäkelä, J. M.: Stable sulphate clusters as a source of new  
680 atmospheric particles, *Nature*, 404, 66–69, <https://doi.org/10.1038/35003550>, 2000.

681 Kulmala, M., Vehkamäki, H., Petäjä, T., Dal Maso, M., Lauri, A., Kerminen, V. M., Birmili, W., and  
682 McMurry, P. H.: Formation and growth rates of ultrafine atmospheric particles: A review of  
683 observations, *J. Aerosol Sci.*, 35, 143–176, <https://doi.org/10.1016/j.jaerosci.2003.10.003>, 2004.

684 Kulmala, M., Petäjä, T., Nieminen, T., Sipilä, M., Manninen, H. E., Lehtipalo, K., Dal Maso, M.,  
685 Aalto, P. P., Junninen, H., Paasonen, P., Riipinen, I., Lehtinen, K. E. J., Laaksonen, A., and  
686 Kerminen, V.-M.: Measurement of the nucleation of atmospheric aerosol particles, *Nat. Protoc.*,  
687 7, 1651–1667, <https://doi.org/10.1038/nprot.2012.091>, 2012.

688 Kulmala, M., Petäjä, T., Ehn, M., Thornton, J., Sipilä, M., Worsnop, D. R., and Kerminen, V. M.:  
689 Chemistry of atmospheric nucleation: On the recent advances on precursor characterization and  
690 atmospheric cluster composition in connection with atmospheric new particle formation, *Annu.*  
691 *Rev. Phys. Chem.*, 65, 21–37, <https://doi.org/10.1146/annurev-physchem-040412-110014>, 2014.

692 Kulmala, M., Kerminen, V.-M., Petäjä, T., Ding, A. J., and Wang, L.: Atmospheric gas-to-particle  
693 conversion: why NPF events are observed in megacities?, *Faraday Discuss.*, 200, 271–288,  
694 <https://doi.org/10.1039/C6FD00257A>, 2017.

695 Kulmala, M., Petäjä, T., Kerminen, V. M., Kujansuu, J., Ruuskanen, T., Ding, A., Nie, W., Hu, M.,  
696 Wang, Z., Wu, Z., Wang, L., and Worsnop, D. R.: On secondary new particle formation in China,  
697 *Front. Environ. Sci. Eng.*, 10, 1–10, <https://doi.org/10.1007/s11783-016-0850-1>, 2016.

698 Kürten, A., Bergen, A., Heinritzi, M., Leiminger, M., Lorenz, V., Piel, F., Simon, M., Sitals, R.,  
699 Wagner, A. C., and Curtius, J.: Observation of new particle formation and measurement of  
700 sulfuric acid, ammonia, amines and highly oxidized organic molecules at a rural site in central  
701 Germany, *Atmos. Chem. Phys.*, 16, 12793–12813, <https://doi.org/10.5194/acp-16-12793-2016>,  
702 2016.

703 Lin, W., Xu, X., Ge, B., and Zhang, X.: Characteristics of gaseous pollutants at Gucheng, a rural site

704 southwest of Beijing, *J. Geophys. Res. Atmos.*, 114, <https://doi.org/10.1029/2008JD010339>,  
705 2009.

706 Liu, S., Hu, M., Wu, Z., Wehner, B., Wiedensohler, A., and Cheng, Y.: Aerosol number size  
707 distribution and new particle formation at a rural/coastal site in Pearl River Delta (PRD) of China,  
708 *Atmos. Environ.*, 42, 6275–6283, <https://doi.org/10.1016/j.atmosenv.2008.01.063>, 2008.

709 Liu, Y., Yan, C., Feng, Z., Zheng, F., Fan, X., Zhang, Y., Li, C., Zhou, Y., Lin, Z., Guo, Y., Zhang, Y., Ma,  
710 L., Zhou, W., Liu, Z., Dada, L., Dällenbach, K., Kontkanen, J., Cai, R., Chan, T., Chu, B., Du, W., Yao,  
711 L., Wang, Y., Cai, J., Kangasluoma, J., Kokkonen, T., Kujansuu, J., Rusanen, A., Deng, C., Fu, Y., Yin,  
712 R., Li, X., Lu, Y., Liu, Y., Lian, C., Yang, D., Wang, W., Ge, M., Wang, Y., Worsnop, D. R., Junninen,  
713 H., He, H., Kerminen, V. M., Zheng, J., Wang, L., Jiang, J., Petäjä, T., Bianchi, F., and Kulmala, M.:  
714 Continuous and comprehensive atmospheric observations in Beijing: a station to understand the  
715 complex urban atmospheric environment, *Big Earth Data*, 4, 295–321,  
716 <https://doi.org/10.1080/20964471.2020.1798707>, 2020.

717 Lu, Y., Yan, C., Fu, Y., Chen, Y., Liu, Y., Yang, G., Wang, Y., Bianchi, F., Chu, B., Zhou, Y., Yin, R.,  
718 Baalbaki, R., Garmash, O., Deng, C., Wang, W., Liu, Y., Petäjä, T., Kerminen, V. M., Jiang, J.,  
719 Kulmala, M., and Wang, L.: A proxy for atmospheric daytime gaseous sulfuric acid concentration  
720 in urban Beijing, *Atmos. Chem. Phys.*, 19, 1971–1983, <https://doi.org/10.5194/acp-19-1971-2019>,  
721 2019.

722 Ma, N., Zhao, C., Tao, J., Wu, Z., Kecorius, S., Wang, Z., Groß, J., Liu, H., Bian, Y., Kuang, Y., Teich,  
723 M., Spindler, G., Müller, K., Van Pinxteren, D., Herrmann, H., Hu, M., and Wiedensohler, A.:  
724 Variation of CCN activity during new particle formation events in the North China Plain, *Atmos.*  
725 *Chem. Phys.*, 16, 8593–8607, <https://doi.org/10.5194/acp-16-8593-2016>, 2016.

726 McMurry, P. H., Fink, M., Sakurai, H., Stolzenburg, M. R., Mauldin, I. L., Smith, J., Eisele, F., Moore,  
727 K., Sjostedt, S., Tanner, D., Huey, L. G., Nowak, J. B., Edgerton, E., and Voisin, D.: A criterion for  
728 new particle formation in the sulfur-rich Atlanta atmosphere, *J. Geophys. Res. Atmos.*, 110, 1–10,  
729 <https://doi.org/10.1029/2005JD005901>, 2005.

730 Mikko Sipilä, Torsten Berndt, Tuukka Petäjä, David Brus, Joonas Vanhanen, Frank  
731 Stratmann, Johanna Patokoski, Roy L. Mauldin III, Antti-Pekka Hyvärinen, Frank Stratmann,  
732 Johanna Patokoski, Roy L. Mauldin III, Heikki Lihavainen, M. K.: The Role of Sulfuric Acid in  
733 Atmospheric Nucleation, *Science* (80-. ), 327, 1243–1246, 2010.

734 Mirme, S. and Mirme, A.: The mathematical principles and design of the NAIS - A spectrometer  
735 for the measurement of cluster ion and nanometer aerosol size distributions, *Atmos. Meas. Tech.*,  
736 6, 1061–1071, <https://doi.org/10.5194/amt-6-1061-2013>, 2013.

737 Mohr, C., Thornton, J. A., Heitto, A., Lopez-Hilfiker, F. D., Lutz, A., Riipinen, I., Hong, J., Donahue,  
738 N. M., Hallquist, M., Petäjä, T., Kulmala, M., and Yli-Juuti, T.: Molecular identification of organic  
739 vapors driving atmospheric nanoparticle growth, *Nat. Commun.*, 10, 4442,  
740 <https://doi.org/10.1038/s41467-019-12473-2>, 2019.

741 Mönkkönen, P., Koponen, I. K., Lehtinen, K. E. J., Hämeri, K., Uma, R., and Kulmala, M.:  
742 Measurements in a highly polluted Asian mega city: observations of aerosol number size  
743 distribution, modal parameters and nucleation events, *Atmos. Chem. Phys. Discuss.*, 4,  
744 5407–5431, <https://doi.org/10.5194/acpd-4-5407-2004>, 2005.

745 Nieminen, T., Lehtinen, K. E. J., and Kulmala, M.: Sub-10 nm particle growth by vapor  
746 condensation-effects of vapor molecule size and particle thermal speed, *Atmos. Chem. Phys.*, 10,  
747 9773–9779, <https://doi.org/10.5194/acp-10-9773-2010>, 2010.

748 Nieminen, T., Asmi, A., Aalto, P. P., Keronen, P., Petäjä, T., Kulmala, M., Kerminen, V. M.,  
749 Nieminen, T., and Dal Maso, M.: Trends in atmospheric new-particle formation: 16 years of  
750 observations in a boreal-forest environment, *Boreal Environ. Res.*, **19**, 191–214, 2014.

751 Petäjä, T., Mauldin, R. L., Kosciuch, E., McGrath, J., Nieminen, T., Paasonen, P., Boy, M., Adamov,  
752 A., Kotiaho, T., and Kulmala, M.: Sulfuric acid and OH concentrations in a boreal forest site,  
753 *Atmos. Chem. Phys.*, **9**, 7435–7448, <https://doi.org/10.5194/acp-9-7435-2009>, 2009.

754 Riccobono, F., Schobesberger, S., Scott, C. E., Dommen, J., Ortega, I. K., Rondo, L., Almeida, J.,  
755 Amorim, A., Bianchi, F., Breitenlechner, M., David, A., Downard, A., Dunne, E. M., Duplissy, J.,  
756 Ehrhart, S., Flagan, R. C., Franchin, A., Hansel, A., Junninen, H., Kajos, M., Keskinen, H., Kupc, A.,  
757 Kürten, A., Kvashin, A. N., Laaksonen, A., Lehtipalo, K., Makhmutov, V., Mathot, S., Nieminen, T.,  
758 Onnela, A., Petäjä, T., Praplan, A. P., Santos, F. D., Schallhart, S., Seinfeld, J. H., Sipilä, M.,  
759 Spracklen, D. V., Stozhkov, Y., Stratmann, F., Tomé, A., Tsagkogeorgas, G., Vaattovaara, P.,  
760 Viisanen, Y., Vrtala, A., Wagner, P. E., Weingartner, E., Wex, H., Wimmer, D., Carslaw, K. S.,  
761 Curtius, J., Donahue, N. M., Kirkby, J., Kulmala, M., Worsnop, D. R., and Baltensperger, U.:  
762 Oxidation products of biogenic emissions contribute to nucleation of atmospheric particles,  
763 *Science (80-. )*, **344**, 717–721, <https://doi.org/10.1126/science.1243527>, 2014.

764 Shen, X., Sun, J., Zhang, X., Zhang, Y., Wang, Y., Tan, K., Wang, P., Zhang, L., Qi, X., Che, H., Zhang,  
765 Z., Zhong, J., Zhao, H., and Ren, S.: Comparison of Submicron Particles at a Rural and an Urban  
766 Site in the North China Plain during the December 2016 Heavy Pollution Episodes, *J. Meteorol.*  
767 *Res.*, **32**, 26–37, <https://doi.org/10.1007/s13351-018-7060-7>, 2018a.

768 Shen, X., Sun, J., Kivekäs, N., Kristensson, A., Zhang, X., Zhang, Y., Zhang, L., Fan, R., Qi, X., Ma, Q.,  
769 and Zhou, H.: Spatial distribution and occurrence probability of regional new particle formation  
770 events in eastern China, *Atmos. Chem. Phys.*, **18**, 587–599,  
771 <https://doi.org/10.5194/acp-18-587-2018>, 2018b.

772 Spracklen, D. V., Carslaw, K. S., Kulmala, M., Kerminen, V. M., Mann, G. W., and Sihto, S. L.: The  
773 contribution of boundary layer nucleation events to total particle concentrations on regional and  
774 global scales, *Atmos. Chem. Phys.*, **6**, 5631–5648, <https://doi.org/10.5194/acp-6-5631-2006>,  
775 2006.

776 Stolzenburg, D., Simon, M., Ranjithkumar, A., Kürten, A., Lehtipalo, K., Gordon, H., Ehrhart, S.,  
777 Finkenzeller, H., Pichelstorfer, L., Nieminen, T., He, X., Brilke, S., Xiao, M., Amorim, A., Baalbaki, R.,  
778 Baccarini, A., and Beck, L.: Enhanced growth rate of atmospheric particles from sulfuric acid,  
779 7359–7372, 2020.

780 Tan, H. B., Yin, Y., Li, F., Liu, X. T., Chan, P. W., Deng, T., Deng, X. J., Wan, Q. L., and Wu, D.:  
781 Measurements of particle number size distributions and new particle formation events during  
782 winter in the Pearl River Delta region, China, *J. Trop. Meteorol.*, **22**, 191–199,  
783 <https://doi.org/10.16555/j.1006-8775.2016.02.009>, 2016.

784 Tröstl, J., Chuang, W. K., Gordon, H., Heinritzi, M., Yan, C., Molteni, U., Ahlm, L., Frege, C., Bianchi,  
785 F., Wagner, R., Simon, M., Lehtipalo, K., Williamson, C., Craven, J. S., Duplissy, J., Adamov, A.,  
786 Almeida, J., Bernhammer, A. K., Breitenlechner, M., Brilke, S., Dias, A., Ehrhart, S., Flagan, R. C.,  
787 Franchin, A., Fuchs, C., Guida, R., Gysel, M., Hansel, A., Hoyle, C. R., Jokinen, T., Junninen, H.,  
788 Kangasluoma, J., Keskinen, H., Kim, J., Krapf, M., Kürten, A., Laaksonen, A., Lawler, M., Leiminger,  
789 M., Mathot, S., Möhler, O., Nieminen, T., Onnela, A., Petäjä, T., Piel, F. M., Miettinen, P., Rissanen,  
790 M. P., Rondo, L., Sarnela, N., Schobesberger, S., Sengupta, K., Sipilä, M., Smith, J. N., Steiner, G.,  
791 Tomè, A., Virtanen, A., Wagner, A. C., Weingartner, E., Wimmer, D., Winkler, P. M., Ye, P.,

792 Carslaw, K. S., Curtius, J., Dommen, J., Kirkby, J., Kulmala, M., Riipinen, I., Worsnop, D. R.,  
793 Donahue, N. M., and Baltensperger, U.: The role of low-volatility organic compounds in initial  
794 particle growth in the atmosphere, *Nature*, 533, 527–531, <https://doi.org/10.1038/nature18271>,  
795 2016.

796 Vanhanen, J., Mikkilä, J., Lehtipalo, K., Sipil, M., Manninen, H. E., Siivola, E., and Petäjä, T.: Particle  
797 Size Magnifier for Nano-CN Detection, *Aerosol Sci. Technol.*, 533–542,  
798 <https://doi.org/10.1080/02786826.2010.547889>, 2011.

799 Varghese, M., Leena, P. P., Murugavel, P., Bankar, S., Todekar, K., Chowdhuri, S., Safai, P. D.,  
800 Malap, N., Konwar, M., Dixit, S., Rao, Y. J., and Prabha, T. V.: New Particle Formation Observed  
801 from a Rain Shadow Region of the Western Ghats India, *Toxicol. Environ. Chem.*, 0, 1–29,  
802 <https://doi.org/10.1080/02772248.2020.1789134>, 2020.

803 Wang, Z., Wu, Z., Yue, D., Shang, D., Guo, S., Sun, J., Ding, A., Wang, L., Jiang, J., Guo, H., Gao, J.,  
804 Cheung, H. C., Morawska, L., Keywood, M., and Hu, M.: New particle formation in China: Current  
805 knowledge and further directions, *Sci. Total Environ.*, 577, 258–266,  
806 <https://doi.org/10.1016/j.scitotenv.2016.10.177>, 2017.

807 Wang, Z. B., Hu, M., Sun, J. Y., Wu, Z. J., Yue, D. L., Shen, X. J., Zhang, Y. M., Pei, X. Y., Cheng, Y. F.,  
808 and Wiedensohler, A.: Characteristics of regional new particle formation in urban and regional  
809 background environments in the North China Plain, *Atmos. Chem. Phys.*, 13, 12495–12506,  
810 <https://doi.org/10.5194/acp-13-12495-2013>, 2013.

811 Xiao, S., Wang, M. Y., Yao, L., Kulmala, M., Zhou, B., Yang, X., Chen, J. M., Wang, D. F., Fu, Q. Y.,  
812 Worsnop, D. R., and Wang, L.: Strong atmospheric new particle formation in winter in urban  
813 Shanghai, China, *Atmos. Chem. Phys.*, 15, 1769–1781, <https://doi.org/10.5194/acp-15-1769-2015>,  
814 2015.

815 Yan, C., Yin, R., Lu, Y., Dada, L., Yang, D., Fu, Y., Kontkanen, J., Deng, C., Garmash, O., Ruan, J.,  
816 Baalbaki, R., Schervish, M., Cai, R., Bloss, M., Chan, T., Chen, T., Chen, Q., Chen, X., Chen, Y., Chu,  
817 B., Dällenbach, K., Foreback, B., He, X., Heikkinen, L., Jokinen, T., Junninen, H., Kangasluoma, J.,  
818 Kokkonen, T., Kurppa, M., Lehtipalo, K., Li, H., Li, H., Li, X., Liu, Y., Ma, Q., Paasonen, P., Rantala, P.,  
819 Pileci, R. E., Rusanen, A., Sarnela, N., Simonen, P., Wang, S., Wang, W., Wang, Y., Xue, M., Yang,  
820 G., Yao, L., Zhou, Y., Kujansuu, J., Petäjä, T., Nie, W., Ma, Y., Ge, M., He, H., Donahue, N. M.,  
821 Worsnop, D. R., Veli-Matti Kerminen, Wang, L., Liu, Y., Zheng, J., Kulmala, M., Jiang, J., and  
822 Bianchi, F.: The Synergistic Role of Sulfuric Acid, Bases, and Oxidized Organics Governing  
823 New-Particle Formation in Beijing, *Geophys. Res. Lett.*, 48, 1–12,  
824 <https://doi.org/10.1029/2020GL091944>, 2021.

825 Yang, L., Nie, W., Liu, Y., Xu, Z., Xiao, M., Qi, X., Li, Y., Wang, R., Zou, J., Paasonen, P., Yan, C., Xu,  
826 Z., Wang, J., Zhou, C., Yuan, J., Sun, J., Chi, X., Kerminen, V. M., Kulmala, M., and Ding, A.: Toward  
827 Building a Physical Proxy for Gas-Phase Sulfuric Acid Concentration Based on Its Budget Analysis  
828 in Polluted Yangtze River Delta, East China, *Environ. Sci. Technol.*, 55, 6665–6676,  
829 <https://doi.org/10.1021/acs.est.1c00738>, 2021.

830 Yao, L., Garmash, O., Bianchi, F., Zheng, J., Yan, C., Paasonen, P., Sipilä, M., Wang, M., Wang, X.,  
831 and Xiao, S.: Atmospheric new particle formation from sulfuric acid and amines in a Chinese  
832 megacity, *Science (80-. )*, 281, 278–281, 2018.

833 Yu, H., Ren, L., and Kanawade, V. P.: New Particle Formation and Growth Mechanisms in Highly  
834 Polluted Environments, *Curr. Pollut. Reports*, 3, 245–253,  
835 <https://doi.org/10.1007/s40726-017-0067-3>, 2017.

836 Yue, D., Hu, M., Wu, Z., Wang, Z., Guo, S., Wehner, B., Nowak, A., Achtert, P., Wiedensohler, A.,  
837 Jung, J., Kim, Y. J., and Liu, S.: Characteristics of aerosol size distributions and new particle  
838 formation in the summer in Beijing, *J. Geophys. Res. Atmos.*, **114**, 1–13,  
839 <https://doi.org/10.1029/2008JD010894>, 2009.

840 Zhang, R., Khalizov, A., Wang, L., Hu, M., and Xu, W.: Nucleation and Growth of Nanoparticles in  
841 the Atmosphere, *Chem. Rev.*, **112**, 1957–2011, <https://doi.org/10.1021/cr2001756>, 2012.

842 Zhang, R., Wang, G., Guo, S., Zamora, M. L., Ying, Q., Lin, Y., Wang, W., Hu, M., and Wang, Y.:  
843 Formation of Urban Fine Particulate Matter, *Chem. Rev.*, **115**, 3803–3855,  
844 <https://doi.org/10.1021/acs.chemrev.5b00067>, 2015.

845 Zhang, Y., Tao, J., Ma, N., Kuang, Y., Wang, Z., Cheng, P., Xu, W., Yang, W., Zhang, S., Xiong, C.,  
846 Dong, W., Xie, L., Sun, Y., Fu, P., Zhou, G., Cheng, Y., and Su, H.: Predicting cloud condensation  
847 nuclei number concentration based on conventional measurements of aerosol properties in the  
848 North China Plain, *Sci. Total Environ.*, **719**, 137473,  
849 <https://doi.org/10.1016/j.scitotenv.2020.137473>, 2020.

850 Zhou, Y., Dada, L., Liu, Y., Fu, Y., Kangasluoma, J., Chan, T., Yan, C., Chu, B., Daellenbach, K. R.,  
851 Bianchi, F., Kokkonen, T. V., Liu, Y., Kujansuu, J., Kerminen, V. M., Petäjä, T., Wang, L., Jiang, J.,  
852 and Kulmala, M.: Variation of size-segregated particle number concentrations in wintertime  
853 Beijing, *Atmos. Chem. Phys.*, **20**, 1201–1216, <https://doi.org/10.5194/acp-20-1201-2020>, 2020.

854